Load Sharing Strategy Incorporating Power Limits in Islanded Inverter-Based Microgrids

Chiebuka Eyisi[*1], Guanyu Tian[*2], Petr Vorobev[β], and Qifeng Li[*3]
[*1, 2, 3] Department of Electrical & Computer Engineering, University of Central Florida, Orlando, FL, USA
[β] Center for Energy Science & Technology, Skolkovo Institute of Science & Technology, Moscow, Russia
Email: [*1] cvpeyisi@knights.ucf.edu, [*2] tiang@knights.ucf.edu, [β] p.vorobev@skoltech.ru, [*3] qifeng.li@ucf.edu

2020 IEEE Electric Power and Energy Conference (EPEC) | 978-1-7281-6489-2/20/$31.00 ©2020 IEEE | DOI: 10.1109/EPEC48502.2020.9320069

***Abstract*—Microgrids (MGs) comprising multiple interconnected distributed energy resources (DERs) with coordinated control strategies can operate in both grid-connected and islanded modes. In the grid-connected mode, the frequency and bus voltages are maintained by the utility grid. In the islanded mode, the DERs maintain the frequency and bus voltages in the MG. This paper presents a load demand sharing strategy in an islanded voltage source inverter-based microgrid (VSI-MG). The survivability of the interconnected MG in the presence of a single fully loaded VSI in an islanded VSI-MG is investigated. The concept of virtual synchronous machines (VSM) that enables the modeling of the VSI to emulate the inertia effect of synchronous machines is applied and then a Jacobian-based approach is formulated that takes into account, the capacity of the VSI. Simulation results are presented to verify the effectiveness of the approach.**

***Index Terms*—AC microgrid, distributed energy resources, droop control, transient stability, virtual synchronous machine (VSM).**

I. INTRODUCTION

Electric power grids are rapidly evolving globally where distributed energy resources (DERs) comprising distributed generation (DG) like solar photovoltaic systems (PV), wind turbine generators (WTG), microturbine generators (MTG), diesel engine generators (DEG), as well as energy storage systems (ESS) like battery energy storage systems (BESS), fuel cells (FC), flywheel energy storage (FES), superconducting magnetic energy storage (SMES), compressed air energy storage (CAES) and super capacitors (SC) are interconnected through a low voltage distribution or a medium voltage transmission network to feed required loads in what constitutes the microgrid (MG) concept [1]–[3]. MGs comprising of controllable loads can operate in both islanded and grid-connected operating modes and have been proven for a few decades now to be beneficial for power systems in terms of reduction in emission, lowered energy costs, enhanced resiliency and reliability, lowered costs of upgrades on system infrastructure, and enhanced power quality and energy efficiency [1], [4].

These DERs are interfaced with voltage source inverters (VSI) which are power electronic converters in the case of AC MGs, that enable interconnection in grid-connected and islanded modes of which researchers have investigated its control and management over the years [5]. Primarily with regards to modeling, stability analyses and operational control of these microgrid systems [6], [7]. Some challenges in either grid-connected or islanded modes include active (P) and reactive (Q) power sharing, low inertia, voltage regulation, uncertainty, transition between modes with resynchronization, protection from internal faults and power balance in the associated network [4], [8], [9]. Through these VSIs, various centralized, decentralized, and distributed control strategies have been proposed to address these challenges, which can be aggregated into a hierarchical control architecture [4], [9]–[12]. Three levels exist within the control hierarchy: primary control, secondary control, and tertiary control. Primary control establishes the sharing of active and reactive power while ensuring the stability of the microgrid. This is done through decentralized droop controllers which tend to deviate steady-state network frequency and bus voltages from their nominal values. Secondary control is employed to minimize these deviations so that these nominal values for network frequency and bus voltages can be returned to. Tertiary control is contingent on energy markets and prices to reach a global economic dispatch, operation scheduling and power regulation over the network [11], [12]. A summary of control objectives, problems, and solutions in MGs can be found in [13].

In MG networks, DGs can be classified as dispatchable or non-dispatchable power units [14]. Non-dispatchable units comprise mainly of intermittent renewable energy-based DGs like PVs and WTGs due to the dependence of their output power on weather conditions and not load demand. These non-dispatchable units are commonly backed up with an ESS technology to alleviate this intermittency [3], [11]. Conversely, dispatchable units like MTGs, DEGs and ESSs can generate controlled power on demand and therefore are able to regulate the network frequency and bus voltages while operating in islanded mode. Non-dispatchable units are out of the scope of this paper [2], [14].

In this paper, a load demand sharing strategy is developed for dispatchable DGs in an islanded MG by adopting the conventional droop control which requires no communication link and is based on local measurements [15]. A variety of load power sharing and control strategies from conventional droop to adaptive/improved droop and a network-based droop were

978-1-7281-6489-2/20/$31.00 ©2020 IEEE

all compared and summarized in [11]. A wider classification of these control and sharing strategies into conventional droop methods, angle droop control methods, voltage-real power droop/frequency-reactive power boost (VPD/FQB) methods, virtual impedance methods, virtual inertia methods, consensus-based methods and others can be found in [8]. Furthermore, a performance evaluation was done to compare the conventional droop control, the generalized droop control, a transient droop control, inverse droop control methods and virtual synchronous machines (VSM) methods in [16]. In summary, most of these methods are offspring of conventional droop methods.

Through existing literature, a majority of the control methods seeking to address load sharing begins with a detailed dynamic modeling of installed components in the MG; the subsequent system of equations are then linearized around stable operating points of which a representation in state-space is derived; then eigenvalue, sensitivity and participation analysis could be done to investigate the small-signal stability. After the assessment of stability conditions, time-domain computer simulations or illustrative experiments are carried out to verify the accuracy of the detailed model and control approach proposed [17]–[21]. These detailed models are usually of a high order and could become computationally burdensome in investigating larger MGs. Hence simplifying assumptions with quasi-stationary approximations or tested conditions following the analysis of the timescale separation between the power control modes and the network modes can be used to develop reduced-order models and assuage the computational burden [22]–[24]. It was later discovered in [25] that even this ratio of timescales would not be sufficient for justifying the exclusion of certain fast states in analyzing small-signal stability and hence new stability certificates were proposed for assessing stability.

From preceding commentary, there is an opportunity to add to an existing gap that investigates how other controllable VSIs participate in load sharing when one or more VSIs has reached or approaches its power capability in an islanded MG. Here, the survivability of the interconnected MG in the presence of a single fully loaded VSI in an all islanded VSI-MG is investigated. One of the earliest investigations into this can be found in [26]. Convergence on the fixed slope defining the droop characteristics was nonexistent, but islanded operation could be transiently possible in the presence of an ESS. Hence, in steady state, even in this "fixed droop" method; the output power limits should be enforced. This led to the development of the "variable droop" method in [27] that provides an additional control block to the "fixed droop" method. An overload mitigation controller is presented in [28] to address issues during an increase in load demand when some or all the grid-forming sources (comprising of VSIs, an ESS and a MTG) become overloaded in a MG. The extra load is transferred to other sources when one or more VSIs are overloaded as a result of rapid reduction in frequency. Should all the grid-forming sources be overloaded, then each source participates in reducing the network frequency before under-frequency load shedding can be triggered to disconnect non-essential loads and ensure the MG's survival. This overload mitigation controller is exhibited by the MTG when its electromagnetic torque exceeds the maximum mechanical torque attainable [28].

There seems to be insufficient studies investigating the survivability of the interconnected MG in the presence of one or more fully loaded VSIs in an all islanded VSI-MG. DGs interfaced with VSIs respond faster than traditional DGs, so during the occurrence of a disturbance, the dynamic response of a VSI-interfaced DG in a MG include microsecond electro-magnetic transient process and millisecond electromechanical transient process [25], [29]. To address the objective of this paper, the concept of virtual synchronous machines (VSM) is employed [30]. This concept emulates the inertia effect of traditional synchronous machines where the filter time constant and droop gain of the droop controller's power feedback can be related directly to the inertia constant and damping factor respectively of a VSM [31]. Inertia is included virtually to the VSI-interfaced DGs by adding swing equation [32]–[34]. With the application of this concept and inclusion of requisite algebraic and electrodynamic equations, a Jacobian-based approach is proposed to constrain the VSIs within their power limits while redistributing load so a new steady-state network frequency and bus voltages can be reached. Stability can be assessed during transients in a similar manner done for conventional power systems [35].

The rest of the paper is organized as follows: Section II presents the set of algebraic and electrodynamic equations that characterize the VSI-MG and shows how the VSM concept can be applied. The Jacobian-based approach is introduced in Section III. In Section IV, results are presented and discussed under different cases imposed on the MG system under study; before making concluding remarks in Section V.

II. Mathematical Modeling For VSI-MG And VSM

A. Inverter, Network and Load Equations

As widely reported in literature, the complete system model including the VSI, the load and the network model is developed in the $d-q$ frame [17]–[25].

1) Inverter Power and Droop Control Equations:

The conventional droop control laws that perform the primary control function for the VSI in an islanded MG can be written as:

$$\omega^* = \omega_{set} - \frac{k_p \omega_0}{S_n} P = \omega_{set} - m_p P \quad (1)$$

$$V^* = V_{set} - \frac{k_q V_0}{S_n} Q = V_{set} - n_q Q \quad (2)$$

where ω_{set} and V_{set} represent the nominal setpoints for frequency and voltage controllers respectively, while $S_n = S_{inv}/S_{base}$ is the rating of the VSI with respect to the base power S_{base}. The nominal per-unit frequency droop gain at the maximum real power is k_p, while the nominal per-unit voltage droop at the maximum reactive power is k_q. These values are typically set within $0.5\% - 3\%$ [17]. The nominal frequency and voltage are set by ω_0 and V_0 respectively. The variables P and Q represent the active and reactive power output of the VSI respectively. To eliminate noise and oscillations, instantaneous active and reactive power values (P_e and Q_e) is filtered through a low pass filter designed with cutoff frequency ω_c, as shown:

$$P = \frac{\omega_c}{s+\omega_c} P_e\,, \quad Q = \frac{\omega_c}{s+\omega_c} Q_e \quad (3)$$

The instantaneous powers (P_e and Q_e) are calculated from measured output voltage (v_{od}, v_{oq}) and current (i_{od}, i_{oq}) signals as shown:

$$P_e = v_{od}i_{od} + v_{oq}i_{oq}\,, \quad Q_e = v_{oq}i_{od} - v_{od}i_{oq}\,. \tag{4}$$

2) Network Equations:

The equations for the line currents connected between buses m and n are as shown:

$$\frac{dI_{line,d,mn}}{dt} = -\frac{R_{line,mn}}{L_{line,mn}} I_{line,d,mn} + \omega_0 I_{line,q,mn} + \frac{(V_{d,m} - V_{d,n})}{L_{line,mn}} \tag{5}$$

$$\frac{dI_{line,q,mn}}{dt} = -\frac{R_{line,mn}}{L_{line,mn}} I_{line,q,mn} - \omega_0 I_{line,d,mn} + \frac{(V_{q,m} - V_{q,n})}{L_{line,mn}} \tag{6}$$

where R_{line}, L_{line} are the line resistance and inductance, $I_{line,d}$, $I_{line,q}$ are the $d-q$ axis line currents, and V_d, V_q are the $d-q$ axis bus voltages respectively.

3) Load Equations:

A general RL load is considered. The equations for the load currents connected at bus m is as shown:

$$\frac{dI_{load,d,m}}{dt} = -\frac{R_{load,m}}{L_{load,m}} I_{load,d,m} + \omega_0 I_{load,q,m} + \frac{V_{d,m}}{L_{load,m}} \tag{7}$$

$$\frac{dI_{load,q,m}}{dt} = -\frac{R_{load,m}}{L_{load,m}} I_{load,q,m} - \omega_0 I_{load,d,m} + \frac{V_{q,m}}{L_{load,m}} \tag{8}$$

where R_{load}, L_{load} are the load resistance and inductance, and $I_{load,d}$, $I_{load,q}$ are the $d-q$ axis load currents respectively.

B. VSM Concept

To emulate the swing equation of synchronous machines for VSIs, the active power droop equation described in (1) and in conjunction with (3) can be rewritten as shown:

$$\omega^* = \omega_{set} - m_p \frac{\omega_c}{s+\omega_c} P \tag{9}$$

An assumption that the output frequency follows the reference frequency $\omega^* = \omega$, can be made since the inner current and voltage loop act fast due to higher bandwidth [32]. Hence, what follows is:

$$\omega = \omega_{set} - m_p \frac{\omega_c}{s+\omega_c} P \tag{10}$$

In differential form, the above equation can be rewritten at bus m, and rearranged as shown:

$$\frac{d\omega_m}{dt} = \frac{1}{\tau_m}\left(\omega_{set,m} - \omega_m - m_{p,m}P_m\right) \tag{11}$$

where $\tau_m = 1/\omega_{c,m}$ is the filter time of the power controller for the VSI at bus m. An analogy can be made between (11) and the swing equation [30], [32]. That inertia J and damping coefficient D, have the following relational proportionality:

$$J \propto \frac{1}{m_p \omega_c \omega_0}\,, \quad D \propto \frac{1}{m_p \omega_0} \tag{12}$$

An analogous function of the virtual inertia is served by the active power first order low pass filter's cutoff frequency, ω_c. The higher the droop gain, the higher the damping and hence mathematically verifying that VSIs contribute more to damping of electromechanical modes [30], [32]. From (11), with the required level of accuracy, the angle can be described using:

$$\frac{d\theta_m}{dt} = \omega_m - \omega_0 \tag{13}$$

By mirroring (11) and using (2) in conjunction with (3), the following equation can be used to characterize the reactive power:

$$\frac{dV_m}{dt} = \frac{1}{\tau_m}\left(V_{set,m} - V_m - n_{q,m}Q_m\right) \tag{14}$$

The following algebraic equations would also be included to complete the emulation of the VSI as a VSM: The active and reactive power generated by a VSI at bus m are:

$$P_m = Re[V_m e^{j\theta_m} \textstyle\sum_{k\in M_m} I^*_{line,mn}] + Re[V_m e^{j\theta_m} I^*_{load,m}] \tag{15}$$

$$Q_m = Im[V_m e^{j\theta_m} \textstyle\sum_{k\in M_m} I^*_{line,mn}] + Im[V_m e^{j\theta_m} I^*_{load,m}] \tag{16}$$

where M_m is the set of bus numbers with a direct connection to bus m, and the following phasor equations below represent the voltage, line, and load currents respectively:

$$V_m = V_{d,m} + jV_{q,m} = V_m e^{j\theta_m} \tag{17}$$

$$I_{line,mn} = I_{line,d,mn} + jI_{line,q,mn} \tag{18}$$

$$I_{load,mn} = I_{load,d,mn} + jI_{load,q,mn} \tag{19}$$

III. Jacobian-Based Approach

A Jacobian-based approach is formulated to keep the VSIs within their maximum power capability so that during a load change, a new steady-state network frequency can be found while redistributing loads in the VSI-MG if one of the VSIs reaches its output power capability. The approach begins by using the equations (5) – (8), (11), (13) and (14) to characterize the dynamic states of the system. Theses states are calculated as functions of time using appropriate numerical procedures. While advancing the states in time, the algebraic equations (15), (16) are monitored for any capacity violations. When a violation occurs, the following equation describing correction terms is constructed at that instant in time:

$$\begin{bmatrix} \Delta\theta_1 \\ \vdots \\ \Delta\theta_k \\ \Delta V_1 \\ \vdots \\ \Delta V_k \end{bmatrix} = \begin{bmatrix} \frac{\partial P_1}{\partial \theta_1} & \cdots & \frac{\partial P_1}{\partial \theta_k} & \frac{\partial P_1}{\partial V_1} & \cdots & \frac{\partial P_1}{\partial V_k} \\ \vdots & \ddots & \vdots & \vdots & \ddots & \vdots \\ \frac{\partial P_k}{\partial \theta_1} & \cdots & \frac{\partial P_k}{\partial \theta_k} & \frac{\partial P_k}{\partial V_1} & \cdots & \frac{\partial P_k}{\partial V_k} \\ \frac{\partial Q_1}{\partial \theta_1} & \cdots & \frac{\partial Q_1}{\partial \theta_k} & \frac{\partial Q_1}{\partial V_1} & \cdots & \frac{\partial Q_1}{\partial V_k} \\ \vdots & \ddots & \vdots & \vdots & \ddots & \vdots \\ \frac{\partial Q_k}{\partial \theta_1} & \cdots & \frac{\partial Q_k}{\partial \theta_k} & \frac{\partial Q_k}{\partial V_1} & \cdots & \frac{\partial Q_k}{\partial V_k} \end{bmatrix}^{-1} \begin{bmatrix} P_{r1}\left(P_1^{limit} - P_1\right) \\ \vdots \\ P_{rk}\left(P_k^{limit} - P_k\right) \\ Q_{r1}\left(Q_1^{limit} - Q_1\right) \\ \vdots \\ Q_{rk}\left(Q_k^{limit} - Q_k\right) \end{bmatrix} \tag{20}$$

where k is the last m-index in the subset k_m, belonging to the set of all network buses M where there is a VSI connected, and the Jacobian matrix includes the partial derivatives of the active and reactive powers given in (15) and (16) with respect to angle and voltage states. For example, in a network with 5 buses represented by the set $M = \{1, 2, 3, 4, 5\}$ and having the subset $k_m = \{2, 3, 5\}$ where a VSI is connected; the first and last entries (1,1) and (k,k) in the Jacobian matrix are $\partial P_2/\partial \theta_2$ and $\partial Q_5/\partial V_5$ respectively. The terms P_{rm} and Q_{rm} are ratio terms given by:

$$P_{rm} = \frac{\sum_m P_m}{P_m}, \quad Q_{rm} = \frac{\sum_m Q_m}{Q_m}, \qquad m \in k_m \qquad (21)$$

With the constructed equation (20); on its rightmost column, only the violation encountered is entered with the rest of the other entries being made to equal zero so that the new correction terms on the left side of equation (20) are computed and used to supplement the requisite states in (13) and (14) at the next iteration in time. What happens next is the collective slow retardation of the states that continue to contribute to the violation encountered. For an active power violation, the angle states contributing to that violation would incur a slightly increasing slope to hold that violation while other VSIs raise their outputs to meet the power generation deficiency in the VSI-MG. The same occurs with a reactive power violation and voltage states. With this approach, the VSIs seek a new network steady-state frequency after the loads have been redistributed. This is the load sharing strategy.

A new steady-state network frequency can be attained if all VSIs in the MG are able to collectively ride through the violation and redistribute loads by respecting the conventional droop control. The conventional droop control method is a "fixed slope" method and all the VSIs in the MG search for this new operating point on their respective slopes without violating its own power capability. The Jacobian-based approach described, aids to this regard.

IV. VSI-MG Test Case Simulation Results

The VSI-MG under study is a 381V, 50 Hz interconnected system and is shown in the Figure 1 below. The parameters for this network and VSI model parameters are given in Table I.

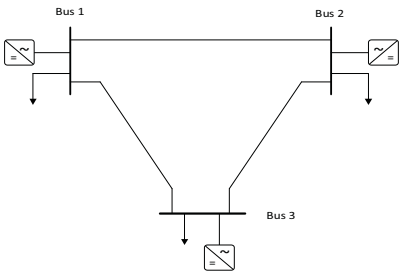

Figure 1. VSI-MG Under Study.

TABLE I. Network And Other Model Parameters

Parameter	Description (Value)
S_{base}	Base Inverter Apparent Power (10 kVA each)
ω_0, V_0	Nominal Frequency (100π rad/s), Nominal Voltage (381 V)
ω_c	Filter Constant (10π rad/s/W)
m_p	$P-\omega$ Droop Gain (3.14e-4 rad/s/W), i.e. k_p (1% at P_{max} = 10 kW)
n_q	$Q-V$ Droop Gain (3.81e-3 V/Var), i.e. k_q (1% at Q_{max} = 10 kVar)
R_{line} , L_{line}	Line Resistance (0.165 Ω/km), Line Inductance (0.26 mH/km)
$line_{mn}$	Line Length in km ($line_{12}$ = 10 , $line_{13}$ = 8 , $line_{23}$ = 6)
$R_{l,1}$, $L_{l,1}$	Bus 1 Load Resistance, Inductance (25 Ω, 19.1 mH)
$R_{l,2}$, $L_{l,2}$	Bus 2 Load Resistance, Inductance (20 Ω, 15.024 mH)
$R_{l,3}$, $L_{l,3}$	Bus 3 Load Resistance, Inductance (40 Ω, 40.0434 mH)

The initial steady-state operating points in per-unit (on 10 kVA, 381 V, 100π rad/s base) were obtained and presented in Table II. The test cases to be investigated are summarized in Table III.

TABLE II. Initial Steady-State Operating Conditions

Parameter	Description (Value)
V_m	Bus 1, 2, 3 Voltages (0.9978, 1.001682, 1.001014)
ω_0	Nominal System Frequency (1.0)
$V_{set,\,m}$	Nominal m-VSI Voltage Setpoints (1.00129752, 1.0020, 1.0012)
$\omega_{set,m}$	Nominal m-VSI Frequency Setpoints (1.0037143, 1.008, 1.004)
θ_m	Bus 1, 2, 3 Voltage Angles in rad (0.0, 0.016849, 0.014305)
$I_{ld,m} + jI_{lq,m}$	Load 1, 2, 3 Currents (0.54780818 – j0.13148365, 0.69131036 – j0.15089985, 0.33202693 – j0.09922594)
$I_{line,d,m} + jI_{line,q,m}$	Line 1-2, 1-3, 2-3 Currents (– 0.08546154 – j0.10617070, – 0.09009769 – j0.11286880, 0.02230564 + j0.02645944)
$P_m + jQ_m$	m-VSI Power Outputs (0.371430 + j0.349752, 0.8000 + j0.031784, 0.4000 + j0.018553)

m – corresponds to the bus number location (1, 2, 3) of the VSI

TABLE III. Test Cases

Case	t = 1 s	t = 2 s	t = 3 s
A	25% ↑ in Load 1	25% ↑ in Load 2	25% ↑ in Load 3
B	25% ↑ in Load 1	50% ↑ in Load 2	25% ↑ in Load 3
C	25% ↑ in Load 1	75% ↑ in Load 2	25% ↑ in Load 3

A. Simulation Results

As seen in Table III, the three cases differ at time, t = 2s. The initial loads in per-unit at bus 1, 2 and 3 using the parameters in Table I are 0.5466 + *j*0.1312, 0.6898 + *j*0.1628 and 0.3309 + *j*0.1041 respectively on a 10 kVA base. With the aid of MATLAB, and application of appropriate numerical procedures in conjunction with the Jacobian-based approach, the following results are presented within.

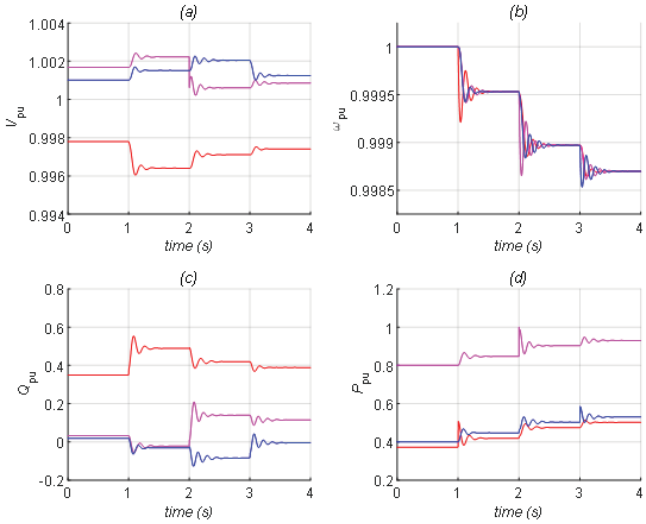

Figure 2. Case A: (a) Bus Voltages, (b) Frequency, (c) Reactive Power Output (d) Active Power Output at VSI Buses (1-red, 2-magenta, 3-blue).

In case A, the VSI at bus 2 is seen in Figure 2(d) to momentarily reach its maximum output active power of 1 p.u. At each time instant when there is a change in load at the bus, the VSI at that bus picks up most of this load change before power sharing occurs between the VSIs. This is the base case to be used in comparison with the other cases B and C.

In case B, where there is a 50% increase in the load at bus 2 instead of the 25% increase seen in case A; the VSIs at all buses are seen to collectively reach a lower steady-state network frequency (0.99813 p.u) compared to case A (0.9987 p.u).

Some noticeable differences in Figure 3(b, d) are seen around t = 2s; where in case B, the equations (11) and (13) for each VSI are amended with the Jacobian matrix so as to stall the increase of active power from the VSI at bus 2, while the other VSIs meet the deficiency in active power generation. Also, there is noticeable longer voltage dip because of the Jacobian matrix amending the voltage at bus 2. At a later time $t \approx 3.1$s, the VSI at bus 2 again momentarily reach its maximum output active power of 1 p.u, but this effect is not as severe as the earlier power violation and all VSIs are able to ride through. In case A, the VSI at the bus of the load change picks up most of the load change, but in case B all three VSIs pick up the load change together when a VSI's power capability is reached.

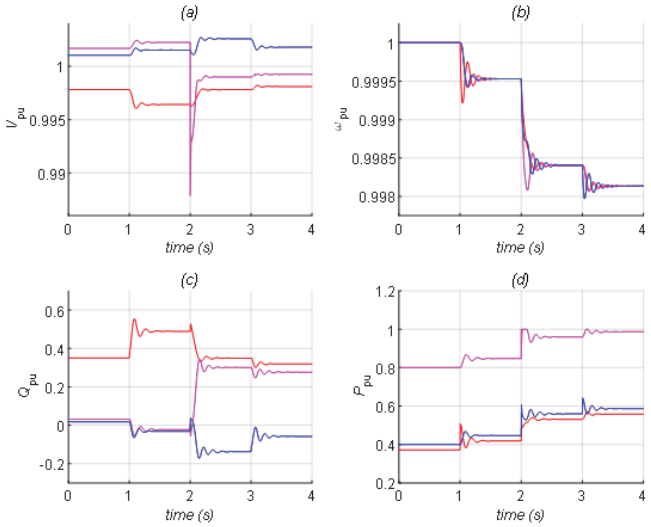

Figure 3. Case B: (a) Bus Voltages, (b) Frequency, (c) Reactive Power Output (d) Active Power Output at VSI Buses (1-red, 2-magenta, 3-blue).

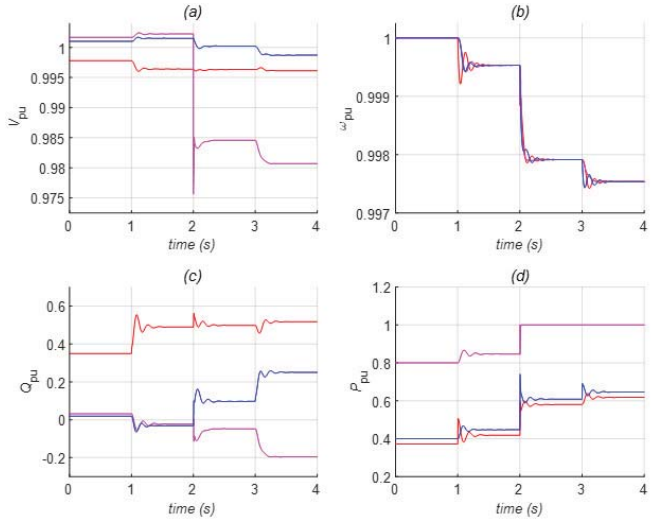

Figure 4. Case C: (a) Bus Voltages, (b) Frequency, (c) Reactive Power Output (d) Active Power Output at VSI Buses (1-red, 2-magenta, 3-blue).

In case C, where there is a 75% increase in the load at bus 2, the system attains a lower steady-state network frequency (0.9975 p.u) among the three VSIs as seen in Figure 4(b). Just like in case B at around t = 2s; the equations (11) and (13) for each VSI are amended with the Jacobian matrix so that when the power capability of the VSI at bus 2 is reached, the other VSIs raise their active power generation to meet this deficiency. The voltage at bus 2 is also amended and constrained to be lower so that the active power limitation imposed by the VSI at bus 2 is accommodated.

B. *Discussion*

To illustrate the differences between the three cases, the figures below show the search path for equilibrium on the $Q - V$ and $P - \omega$ droop control characteristics.

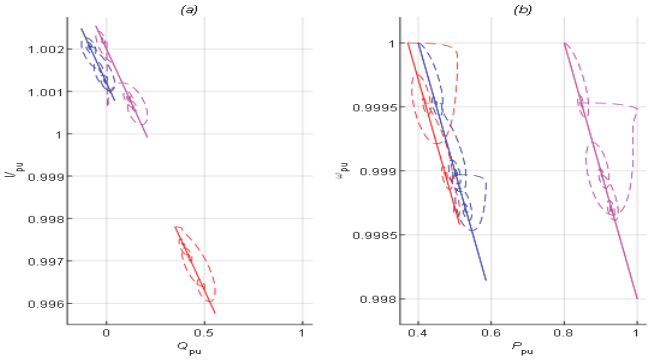

Figure 5. Case A: (a) Q – V Droop Relation, (b) P – ω Droop Relation for VSIs at Buses (1-red, 2-magenta, 3-blue).

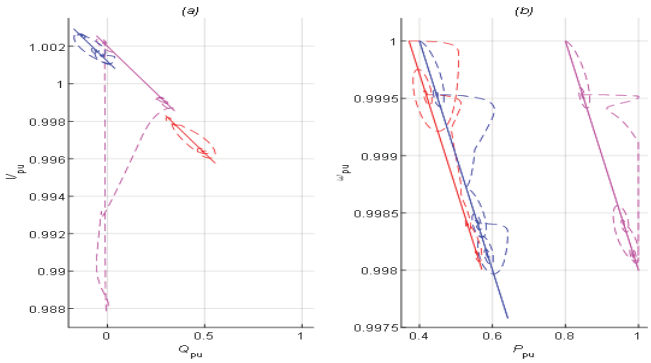

Figure 6. Case B: (a) Q – V Droop Relation, (b) P – ω Droop Relation for VSIs at Buses (1-red, 2-magenta, 3-blue).

The active and reactive power capability of all VSIs are set at 1 p.u and while integrating the state equations with time, the Jacobian-based approach plays the role of preventing each VSI from exceeding this power limitation. What differs in all three cases is the performance of the droop controllers. The $P - \omega$ droop controllers in case A and B as shown in Figures 5(b) and 6(b) respectively see the sustenance of the power limit imposed by the VSI at bus 2 for load changes at $t \geq 2$s. In case C, the $P - \omega$ droop controller in Figure 7(b) sustains the power limitation while correction terms from the Jacobian-based approach lowers the frequency of the VSI at bus 2 in order to enable a new steady-state network frequency to be attained as in Figure 4(b). The $Q - V$ droop control characteristics are also presented, and cases A and B show convergence on its characteristics while case C is amended to accommodate the active power limitation imposed by the VSI at bus 2.

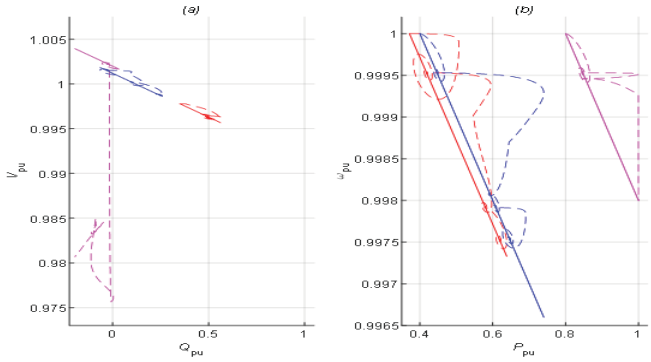

Figure 7. Case C: (a) Q – V Droop Relation, (b) P – ω Droop Relation for VSIs at Buses (1-red, 2-magenta, 3-blue).

V. CONCLUSION

In this study, simulations are shown to verify the effectiveness of the proposed Jacobian-based approach to redistribute loads between the VSIs in a VSI-MG when a single VSI has reached its maximum power capability. Three cases are shown at different loading conditions and the proposed approach is able to assess the survivability of the VSI-MG via their respective conventional droop characteristics.

REFERENCES

[1] R. H. Lasseter, "Microgrids", in *Proc. IEEE Power Engineering Society Winter Meeting*, pp. 305-308, Jan. 2002.

[2] S. Sen and V. Kumar, "Microgrid modelling: a comprehensive survey", *Annual Reviews in Control*, 2018; 46:216-250.

[3] A. A. K. Arani, G. B. Gharehpetian and M. Abedi, "Review on energy storage systems control methods in microgrids", *International Journal of Electrical Power & Energy Systems*, 2019; 107:745-757.

[4] S. Parhizi, H. Lotfi, A. Khodaei and S. Bahramirad, "State of the art in research on microgrids: a review", *IEEE Access*, vol. 3, pp. 890-925.

[5] S. Sen and V. Kumar, "Microgrid control: a comprehensive survey", *Annual Reviews in Control*, 2018; 45:118-151.

[6] M. Farrokhabadi et. al, "Microgrid stability definitions, analysis and examples", *IEEE Trans. on Power Systems*, vol. 35, no. 1, pp. 13-29, Jan. 2020.

[7] J. Schiffer et. al, "A survey on modeling of microgrids–from fundamental physics to phasors and voltage sources", *Automatica*, 2016; 74:135-150.

[8] S. K. Sahoo, A. K. Sinha and N. K. Kishore, "Control techniques in ac, dc, and hybrid ac-dc microgrid: a review", *IEEE Journal of Emerging & Selected Topics in Power Electronics*, vol. 6, no. 2, pp. 738-759, Jun. 2018.

[9] D. E. Olivares et. al, "Trends in microgrid control", *IEEE Trans. on Smart Grid*, vol. 5, no. 4, pp. 1905-1919, Jul. 2014.

[10] H. Han et. al, "Review of power sharing control strategies for islanding operations of ac microgrids", *IEEE Trans. on Smart Grid*, vol. 7, no. 1, pp. 200-215, Jan. 2016.

[11] Y. Han, H. Li, P. Shen, E. A. E. Coelho and J. M. Guerrero, "Review of active and reactive power sharing strategies in hierarchical controlled microgrids", *IEEE Trans. on Power Electronics*, vol. 32, no. 3, pp. 2427-2451, Mar. 2017.

[12] J. M. Guerrero, M. Chandorkar, T-L. Le and P. C. Loh, "Advanced control architectures for intelligent microgrids–Part I: decentralized and hierarchical control", *IEEE Trans. on Industrial Electronics*, vol. 60, np. 4, pp. 1254-1262, Apr. 2013.

[13] B. M. Eid, N. A. Rahim, J. Selvaraj and A. H. El Khateb, "Control methods and objectives for electronically coupled distributed energy resources in microgrids: a review", *IEEE Systems Journal*, vol. 10, no. 2, pp. 446-458, Jun. 2016.

[14] S-J. Ahn et. al, "Power sharing method of multiple distributed generators considering control modes and configurations of a microgrid", *IEEE Trans. on Power Delivery*, vol. 25, no. 3, pp. 2007-2016, Jul. 2010.

[15] M. C. Chandorkar, D. M. Divan and R. Adapa, "Control of parallel connected inverters in standalone ac supply systems", *IEEE Trans. on Industry Applications*, vol. 29, no. 1, pp. 136-143, Jan. 1993.

[16] A. S. Vijay, D. K. Dheer, A. Tiwari and S. Doolla, "Performance evaluation of homogenous and heterogenous droop-based systems in microgrid–stability and transient response perspective", *IEEE Trans. on Energy Conversion*, vol. 34, no. 1, pp. 36-46, Mar. 2019.

[17] N. Pogaku, M. Prodanovic and T. C. Green, "Modeling, analysis and testing of autonomous operation of an inverter-based microgrid", *IEEE Trans. on Power Electronics*, vol. 22, no. 2, pp. 613-625, Mar. 2007.

[18] Y. A-R. I. Mohamed and E. F. El-Saadany, "Adaptive decentralized droop controller to preserve power sharing stability of paralleled inverters in distributed generation microgrid", *IEEE Trans. on Power Electronics*, vol. 23, no. 6, pp. 2806-2816, Nov. 2008.

[19] N. Bottrell, M. Prodanovic and T. C. Green, "Dynamic stability of a microgrid with an active load", *IEEE Trans. on Power Electronics*, vol. 28, no. 11, pp. 5107-5119, Nov. 2013.

[20] M. Rasheduzzaman, J. A. Mueller and J. W. Kimball, "An accurate small-signal model of inverter-dominated islanded microgrids using *dq* reference frame", *IEEE Journal of Emerging and Selected Topics in Power Electronics*, vol. 2, no. 4, pp. 1070-1080, Dec. 2014.

[21] A. Aderibole, H. H. Zeineldin, M. S. El-Moursi, J. C-H. Peng and M. A. Hosani, "Domain of stability characterization for hybrid microgrids considering different power sharing conditions", *IEEE Trans. on Energy Conversion*, vol. 33, no. 1, pp. 312-323, Mar. 2018.

[22] L. Luo and S. V. Dhople, "Spatiotemporal model reduction of inverter-based islanded microgrids", *IEEE Trans. on Energy Conversion*, vol. 29, no. 4, pp. 823-832, Dec. 2014.

[23] I. P. Nikolakakos, H. H. Zeineldin, M. S. El-Moursi and N. D. Hatziargyriou, "Stability evaluation of interconnected multi-inverter microgrids through critical clusters", *IEEE Trans. on Power Systems*, vol. 31, no. 4, pp. 3060-3072, Jul. 2016.

[24] M. Rasheduzzaman, J. A. Mueller and J. W. Kimball, "Reduced-order small-signal model of microgrid systems", *IEEE Trans. on Sustainable Energy*, vol. 6, no. 4, pp. 1292-1305, Oct. 2015.

[25] P. Vorobev, P-H. Huang, M. A. Hosani, J. L. Kirtley and K. Turitsyn, "High-fidelity model order reduction for microgrids stability assessment", *IEEE Trans. on Power Systems*, vol. 33, no. 1, pp. 874-887, Jan. 2018.

[26] P. Piagi and R. H. Lasseter, "Autonomous control of microgrids", in *Proc. IEEE Power Engineering Society General Meeting*, pp. 1-8, Oct. 2006.

[27] H-K. Kang, S-J. Ahn and S-I. Moon, "A new method to determine the droop of inverter-based DGs", in *Proc. IEEE Power and Energy Society General Meeting*, pp. 1-6, Oct. 2009.

[28] W. Du, R. H. Lasseter and A. S. Khalsa, "Survivability of autonomous microgrid during overload events", *IEEE Trans. on Smart Grid*, vol. 10, no. 4, pp. 3515-3524, Jul. 2019.

[29] Z. Shuai et. al, "Microgrid stability: classification and a review", *Renewable and Sustainable Energy Reviews*, 2016; 58:167-179.

[30] S. D'Arco and J. A. Suul, "Virtual synchronous machines–classification of implementations and analysis of equivalence to droop controllers for microgrids", in *Proc. IEEE Grenoble Conference*, pp. 1-7, Jun. 2013.

[31] H-P. Beck and R. Hesse, "Virtual synchronous machine", in *Proc. 9th Int. Conf. on Electrical Power Quality and Utilisation*, pp. 1-6, Oct. 2007.

[32] N. Soni, S. Doolla and M. C. Chandorkar, "Inertia design methods for islanded microgrids having static and rotating energy sources", *IEEE Trans. on Industry Applications*, vol. 52, no. 6, pp. 5165-5174, Nov./Dec. 2016.

[33] Q-C. Zhong and G. Weiss, "Synchronverters: inverters that mimic synchronous generators", *IEEE Trans. on Industrial Electronics*, vol. 58, no. 4, pp. 1259-1267, Apr. 2011.

[34] J. Liu, Y. Miura and T. Ise, "Comparison of dynamic characteristics between virtual synchronous generator and droop control in inverter-based distributed generators", *IEEE Trans. on Power Electronics*, vol. 31, no. 5, pp. 3600-3611, May 2016.

[35] N. Mohan, *Electric Power Systems: A First Course*. Hoboken, NJ, USA: Wiley, 2012.